Data-Driven Analysis of Locomotion for a Class of Articulated Mobile Robots

Data Driven Analysis of Locomotion for a Class of Articulated Mobile Robots

Luca Carbonari
Department of Mechanical
and Aerospace Engineering
Politecnico di Torino
Torino, Italy 10129
Email: luca.carbonari@polito.it

Andrea Botta
Department of Mechanical
and Aerospace Engineering
Politecnico di Torino
Torino, Italy 10129
Email: andrea.botta@polito.it

Paride Cavallone
Department of Mechanical
and Aerospace Engineering
Politecnico di Torino
Torino, Italy 10129
Email: paride.cavallone@polito.it

Luigi Tagliavini
Department of Mechanical
and Aerospace Engineering
Politecnico di Torino
Torino, Italy 10129
Email: luigi.tagliavini@polito.it

Giuseppe Quaglia*
Department of Mechanical
and Aerospace Engineering
Politecnico di Torino
Torino, Italy 10129
Email: giuseppe.quaglia@polito.it

In the recent past, the use of autonomous vehicles is becoming of relevant interest in several fields of application. In many cases, the use of articulated structures is preferred to single chassis robots for their peculiar modularity. Such vehicles are often built as an active front module and a rear one that is pulled passively or that can contribute to the vehicle traction when required. Understanding whether this contribution is convenient or not is the main matter of this paper. Two different mobile robots of different scale and purpose are taken into consideration. A dynamic model is presented and analysed. An experimental validation of the model parameters is also presented in order to make it exploitable as a reliable analysis tool. At last, a simple yet effective actuation law is tested for both the considered robots to evaluate whether the contribution of the back module is beneficial or not to the whole machine manoeuvrability.

1 Introduction

The use of mobile robots is spreading in many fields of applications, due to their peculiar ability to relocate services and tools within their work environment [1, 2]. This skill is strongly related to the ability of the robots to engage spaces extremely different one from another. Usually, specific designs are required to achieve specific needs in particular work-spaces: soil unevenness, dimension, and presence of obstacles are just some of the features that need to be assessed in order to make a mobile autonomous platform as much as possible effective and self-sufficient in its workspace. Among the design structures already proposed by the research community [3, 4], the class of articulated wheeled mobile robots captured a special interest due to their inherent modularity and versatility. Such machines are composed of two (or more than two) modules, functionally identical from the point of view of mobility, and that can be devoted to different tasks. The literature in the field is rich, and many interesting prototypes were developed already, or are object of present studies. The robots Epi.q [5, 6] and Agri.q [7, 8], developed at Politecnico di Torino, are two examples of articulated robots, the former designed for surveillance tasks, while the latter for precision agriculture tasks. Although the two robots are built with extremely different scales (Epi.q is a small scale robot of about $5\,kg$ and $30\,cm$ length, while Agri.q weights $100\,kg$ and is $2\,m$ long), these two machines share a common kinematic functional architecture. Also at Politecnico, Quaglia et al. proposed an innovative low-cost robot for rescue operations [9, 10]. Kimura and Hirose proposed

*Address all correspondence to this author.

a snake-like articulated robot in [11] able to climb obstacles higher than the diameter of its wheels. In [12] Tanaka et al. developed a stair climbing articulated robot, controlled with a follow-the-leader-method.

The locomotion of articulated robots is usually borne by the front module, while the other ones are pulled. In some cases, especially for robots with more than two modules, the traction effort is distributed among all of the components. A lot of work has been done in the field of controlling articulated robots [13, 14], even if most part of the research was dedicated at the complex kinematic motion planning issues deriving from backwards motion and obstacle avoidance [15–17]. The interest around snake-like wheeled mobile robots also pushed the study on simulation and control [18–20].

In parallel to the development of new control strategies, researchers also proposed several models of increasing complexity in order to describe and predict how a robot, or a class of robots, should behave and to optimize controllers. The modelling of such systems is not new, and many works have focused on the main type of mobile robots composed of a single module, such as differential drive robots [21]. Fewer studies go into detail about multi-modular vehicles. Corke and Ridley [22] worked on the steering kinematics of multi modular robots, Ali addressed the dynamic modelling of wheeled robots [23], Classens et al. approached the dynamics of snake like machines [24]. Therefore, these models are not suited to describe robots having very fast dynamics or operating off-road or, more in general, in conditions where significant longitudinal or lateral wheel slips can occur.

In this scenario, this paper develops a dynamic nonholonomic model of a generic articulated eight wheels mobile robot, to be employed as a simulated test-bench for locomotion strategies. After a formal analysis of the traction forces effects, the model is experimentally validated and used to depict the behaviour of the Epi.q and the Agri.q prototypes (which are briefly introduced in the following) when a back actuation is used.

2 The Epi.q and the Agri.q mobile robots

In this section, the two robots main object of the present work are presented and compared. The two prototypes of Epi.q and Agri.q are shown in Fig. 1 and Fig. 2 respectively. Although their extremely different appearance, the functional scheme from which they are derived is very similar, as widely argued in the remainder of the manuscript.

For the design of the Epi.q robot (Fig. 1-a), a modular approach was applied to obtain a flexible structure that can be adapted to different tasks or requirements. The robot is provided with four driving units, each one carrying three wheels whose actuation is synchronous and widely described in past works [5, 6]. In a few words, the robot wheels are connected with three planetary gears while the motor actuates the solar gear. The carrier of the driving unit acts as the planetary gears frame and it is free to rotate around its axis, which coincides to that of the motor. Then, each locomotion unit owns two degrees of freedom and it is able to self-reconfigure de-

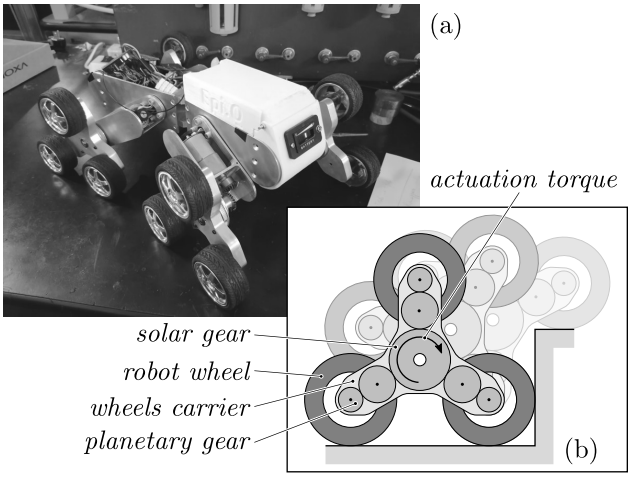

Fig. 1. (a) Latest version of the Epi.q mobile robot and (b) functional scheme of its transmission units.

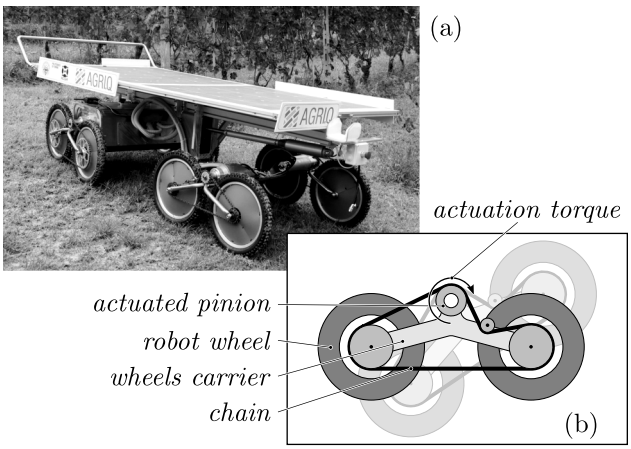

Fig. 2. The Agri.q mobile robot for precision agriculture tasks

pending on the constraint scheme in place, as illustrated in Fig. 1-b. In particular, during motion on flat surfaces, the robot weight constrains the wheels carriers to contact the ground without rotating around their own axes. When the robot bumps into an obstacle, the carriers revolution starts automatically. This brings another wheel in contact with the upper surface of the obstacle, enabling the robot to climb unexpected obstacles with no external commands or actions.

The main guideline which drove the functional design of the Agri.q robot (Fig. 2-a) has been locomotion efficiency on uneven terrains. The Agri.q traction system is conceived to reach a convenient balance between the efficiency of wheels and the effectiveness of tracks on uneven terrains, under both energetic and mobility points of view. To this aim, the rover is provided with four driving units, each one composed of two wheels housed on a rocker arm. For further details on the robot structure, the interested reader is addressed to [7, 8].

The connections of each rocker with the robot main body takes place by means of a passive revolute joint, whose free rotation allows the wheels to follow the ground slopes independently from the configurations of the other rockers. The high number of contact points with the ground ensures a weight distribution similar to that of a tracked robot, while

maintaining an efficiency closer to that of a wheeled machine. The actuators of the modular locomotion systems have been carefully chosen considering, as the most burdening condition, a slope of about 15° to be overcome with only two front traction motors (namely the two front driving units) at a maximum speed of about $5\,km/h$. To achieve such goal, the transmission of each unit is composed of an electric DC motor, connected to a planetary gearbox. In order to synchronously transmit the rotation to the wheels attached to the same rocker, a chain system was used (see Fig. 2-b) which also adds a further velocity reduction and a consequent increase of the available wheel torque. The powertrain layout is completed by a battery able to feed the adopted locomotion systems, and by a solar panel whose dimension has been reasonably chosen to ensure the recharge of the battery during the idle time between missions.

In order to achieve an effective solar tracking, the rover can take advantage of two expressly conceived degrees of freedom able to orientate the upper platform around two independent axes. In particular, the pitch and the roll angles of the solar panel can be modified in a range of respectively $-5°/+40°$ and $-20°/+20°$. Aside the optimization of solar energy harvesting, the pitch and roll degrees of rotation of the upper plane also gives Agri.q a peculiar feature, which is that of providing a an always flat landing surface for drones. The rover, in fact, has been conceived for cooperation with *unmanned aerial vehicles*, UAV's, to offer a capillary monitoring of vineyards.

Although the relevant scale difference, the two robots differ for very few functional details:

- *position of the central joint*: the two robots are characterized by a different aspect ratio $l_f/(l_f+l_b)$, i.e. a different position of the connection joint between the front and the back module. As it is discussed later, such difference significantly affects the dynamic behaviour of the two robots from the actuation strategy point of view;
- *wheels number*: the Epi.q is a small indoor articulated robot, specifically thought to overpass obstacles of different dimension and nature; Agri.q is an agricultural rover, whose traction system has been optimized to assess soil unevenness. For such reason, the small Epi.q has been equipped with a a total number of twelve actuated wheels, three for each driving unit to improve its climbing ability. Nonetheless, during normal use both the robots can rely on eight wheels contemporary in contact with the ground;
- *back module actuation*: while the Epi.q back wheels are able to exert torque in any direction of rotation, many reasons yield the designers to provide the back module of the Agri.q with a uni-lateral transmission similar to that common bicycles are provided with. In first place, such peculiarity significantly improves the battery duration performance of the whole robot for it avoids the transmission gearboxes of the back units being pulled by the rover motion with a consequent efficiency enhancement.

Bearing in mind the peculiarities and the differences of Epi.q and Agri.q, the next sections depict a general dynamics model able to trace the actual behaviour of the two robots after identification of the respective parameters.

Table 1. Relevant geometrical parameters of Epi.q and Agri.q

Parameter	Epi.q	Agri.q	
l_f	0.132	0.000	$[m]$
l_b	0.139	1.300	$[m]$
$l_f/(l_f+l_b)$	0.487	0.000	$[-]$
$i_{x,f}, i_{x,b}$	0.104	0.440	$[m]$
$i_{y,f}, i_{y,b}$	0.260	0.845	$[m]$
r_w	0.032	0.195	$[m]$

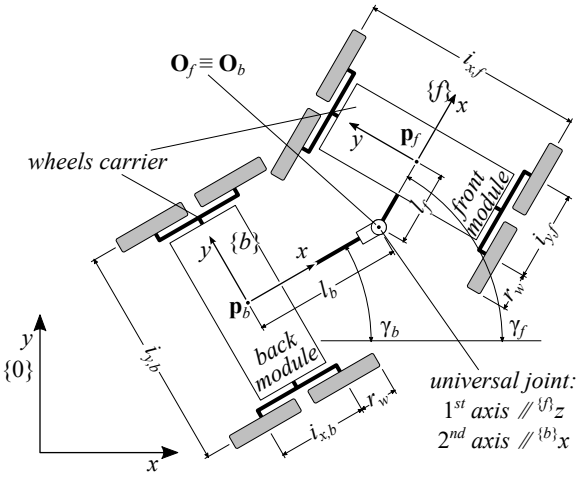

Fig. 3. Kinematic scheme and geometrical parameters of a general eight wheeled articulated mobile robot

3 Kinematics of the Articulated Mobile Robots

The eight wheeled robots kinematic structure is shown in Fig. 3 in a planar simplified representation. Each one of the two modules is characterized by a couple of driving units. Each driving unit has two wheels in contact with the ground. Due to the high number of contact points, and to the non-negligible slips to whom the wheels are subject, a purely kinematic approach hardly fits the actual behaviour of these robots. Therefore, with the aim of analysing the kinematic and dynamic behaviour of this class of machines, a non-holonomic model is presented in the remainder of the manuscript. The geometrical parameters that are used for the modelling process are introduced here, and specialized in the next sections for the two prototypes Epi.q and Agri.q.

The position of the two modules, front and back, are described by means of two reference frames (*r.f.*'s in the following), called $\{f\}$ and $\{b\}$ respectively. The origins of the frames are both located at the intersection between the axis of rotation of the driving units carriers with the longi-

tudinal axis. The $r.f.$'s are oriented so that the x direction is aligned to the longitudinal axis of the modules and the z axis is the ascendant vertical direction (perpendicular to the plane of motion). Therefore, the y axis coincides with the transversal direction and is directed towards the left driving units. The pose of $\{f\}$ and $\{b\}$ is determined by a set of six parameters each, three for position and three for orientation. The positions of the $r.f.$'s are indicated by two vectors $\mathbf{p}_\sim$ composed of:

$$\mathbf{p}_\sim = \begin{bmatrix} x_\sim & y_\sim & z_\sim \end{bmatrix}^T \tag{1}$$

where the symbol $\sim$ stands for f and b for the front and back module respectively.

The orientation of the two modules must be considered carefully. The architecture of the articulated robots does not allow rotations around the longitudinal and transversal axes (x and y directions of $\{f\}$ and $\{b\}$) during motions on planar surfaces. Nonetheless, such rotations are responsible of non-symmetric distributions of wheels loads on the right and left side of the rover, thus the kinematics model cannot disregard their effect. To such aim, the orientation is described by a x-y-z rotation about the axes of the global $r.f.\{0\}$:

$$\mathbf{R}_\sim = \mathbf{R}_{z,\gamma_\sim}\mathbf{R}_{y,\beta_\sim}\mathbf{R}_{x,\alpha_\sim} \tag{2}$$

where $\alpha_\sim$, $\beta_\sim$ and $\gamma_\sim$ are the roll, pitch and yaw angles respectively of the $\sim$ module. The resulting rotation matrix is simplified later by assuming small rotations $\alpha_\sim$ and $\beta_\sim$.

In order to provide a reliable and substantially simplified model, the kinematics of the wheels were simplified as well. In particular, they were considered always in contact with ground while the motions of the wheels carriers were disregarded. As shown later, the inertial contribution of both wheels and carriers have been taken into consideration, yet their mobility have been constrained to the respective module.

4 General Non-Holonomic Dynamics Model

The dynamics of the articulated mobile robots was tackled through a Lagrangian approach. To keep the kinematics formulation as simple as possible, the model was build using Lagrangian multipliers to constraint the front and the back modules by a universal joint. However, given the non negligible slipping of the wheels, the soil-tyre contact was modelled only by means of the exerted forces. In other words, the implemented model is:

$$\frac{d}{dt}\left(\frac{\partial \mathcal{L}}{\partial \dot{\mathbf{x}}}\right) - \frac{\partial \mathcal{L}}{\partial \mathbf{x}} + \mathbf{\Phi}_\mathbf{x}\boldsymbol{\lambda} = \sum \mathbf{Q}_\star \tag{3}$$

where:

- $\mathcal{L}$ is the Lagrangian function of the system, computed as the difference among kinetic and potential energy;
- $\mathbf{x}$ is the vector fo generalized coordinates defining the space of the configurations of the mechanical system whose punctual definition is provided later;
- $\mathbf{\Phi}_\mathbf{x}$ is the Jacobian of the homogeneous constrain equations deriving from the kinematic joints in the mechanical system;
- $\boldsymbol{\lambda}$ is the vector of the Lagrangian multipliers
- $\mathbf{Q}_\star$ is the vector of the generalized forces exchanged by the $\star$ wheel on each coordinate; the meaning and the values of $\mathbf{Q}_\star$ are discussed later, as the wheel contact model is introduced.

4.1 Kinetic and Potential Energies

In this section, the Lagrangian function $\mathcal{L}$ is calculated as:

$$\mathcal{L} = \sum_{\sim=f,b} T_\sim - V \tag{4}$$

where $T_\sim$ is the kinetic energy of the front and back modules, and V is gravity potential forces acting on the system bodies.

The kinetic energy of the front and back modules are obtained as:

$$T_\sim = \frac{1}{2}\dot{\mathbf{p}}_\sim^T m_\sim \dot{\mathbf{p}}_\sim + \frac{1}{2}\boldsymbol{\omega}_\sim^T \mathbf{J}_\sim \boldsymbol{\omega}_\sim \tag{5}$$

where $m_\sim$ is mass of the $\sim$ module and $\mathbf{J}_\sim$ is the inertia matrix with respect to the fixed $r.f.\{0\}$, i.e $\mathbf{J}_\sim = \mathbf{R}_\sim {}^{\{\sim\}}\mathbf{J}_\sim \mathbf{R}_\sim^T$ with ${}^{\{\sim\}}\mathbf{J}_\sim$ being the diagonal principal inertia matrix of the module. For the sake of simplicity, given the smallness of rotations $\alpha_\sim$ and $\beta_\sim$, the inertia matrix can be modified by using only the yaw rotation $\gamma_\sim$, thus:

$$\mathbf{J}_\sim = \mathbf{R}_{z,\gamma_\sim} \mathrm{diag}\left(\mathrm{J_{x,\sim}}, \mathrm{J_{y,\sim}}, \mathrm{J_{z,\sim}}\right) \mathbf{R}_{z,\gamma_\sim}^T \tag{6}$$

Also for simplification purpose, the modules centres of mass are supposed located at the origin of the respective $r.f.\{\sim\}$. The two velocity vectors $\dot{\mathbf{p}}_\sim$ and $\dot{\boldsymbol{\omega}}_\sim$ can be worked out easily by differentiation:

$$\dot{\mathbf{p}}_\sim = \begin{bmatrix} \dot{x}_\sim \\ \dot{y}_\sim \\ \dot{z}_\sim \end{bmatrix} \quad \boldsymbol{\omega}_\sim = \begin{bmatrix} \dot{\alpha}_\sim \cos\beta_\sim \cos\gamma_\sim - \dot{\beta}_\sim \sin\gamma_\sim \\ \dot{\alpha}_\sim \cos\beta_\sim \sin\gamma_\sim + \dot{\beta}_\sim \cos\gamma_\sim \\ \dot{\gamma}_\sim - \dot{\alpha}_\sim \sin\beta_\sim \end{bmatrix} \tag{7}$$

If small pitch and roll rotations are considered, the angular velocity $\boldsymbol{\omega}_\sim$ simplifies as:

$$\boldsymbol{\omega}_\sim = \begin{bmatrix} \dot{\alpha}_\sim \cos\gamma_\sim - \dot{\beta}_\sim \sin\gamma_\sim \\ \dot{\alpha}_\sim \sin\gamma_\sim + \dot{\beta}_\sim \cos\gamma_\sim \\ \dot{\gamma}_\sim \end{bmatrix} \tag{8}$$

The contributions to the kinetic energy provided by the wheels attached to the module is worth a little discussion.

Table 2. Relevant inertial parameters of Epi.q and Agri.q

Parameter	Epi.q	Agri.q	
m_f^*	1.98	59.0	$[kg]$
m_b^*	1.98	28.0	$[kg]$
$J_{f,x}$	0.7×10^{-2}	5.729	$\left[kgm^2\right]$
$J_{f,y}$	1.7×10^{-2}	5.729	$\left[kgm^2\right]$
$J_{f,z}$	0.2×10^{-2}	9.167	$\left[kgm^2\right]$
$J_{b,x}$	0.7×10^{-2}	2.604	$\left[kgm^2\right]$
$J_{b,y}$	1.7×10^{-2}	2.604	$\left[kgm^2\right]$
$J_{b,z}$	0.2×10^{-2}	4.167	$\left[kgm^2\right]$
$J_{w,x} = J_{w,z}$	2.94×10^{-4}	0.155	$\left[kgm^2\right]$
$J_{w,y}$	0.72×10^{-4}	0.038	$\left[kgm^2\right]$

Part of their contribution, in fact, is related to the kinematics of the module itself for they share the same velocity if the motion of the carrier is disregarded. Then, it is possible to consider modified values for the inertial parameters of the front and back chassis so that:

$$\begin{aligned} m^*_{\sim} &= m_{\sim} + 4m_w \\ J^*_{x,\sim} &= J_{x,\sim} + 4J_{w,x} + 2m_w i^2_{y,\sim} \\ J^*_{z,\sim} &= J_{z,\sim} + 4J_{w,z} + 2m_w \left(i^2_{x,\sim} + i^2_{y,\sim}\right) \end{aligned} \tag{9}$$

where m_w is the wheels mass, $J_{w,x}$ and $J_{w,z}$ are the components of the inertia matrix calculated with respect to a $r.f$ centered at the wheel centre of mass, and oriented as $\{\sim\}$; the geometry parameters $i_{x,\sim}$ and $i_{y,\sim}$ respectively represent the transverse and longitudinal dimension of the robot footprint, as shown in Fig. 3. All the wheels have been considered identical to this aim. It is worth remarking that, given the simplified kinematics assumed for the wheels carriers, the model actually disregards the possibility that the wheels attached to a carrier might move differently. This is an acceptable assumption from the point of view of kinetic energy, although it may become relevant in terms of the vertical force exerted by each wheel on the ground. This aspect is presently under investigation, even if the results that are shown later prove that such simplification do not prevent the model to precisely follow the experimental data.

The rotation of the wheels around their own axes is discussed later, for they are relevant for the transmission model that has been implemented. In the specific case of eight wheeled mobile robots, the soil-tyre contact model plays a crucial role in the forces exerted by the machine. Such forces affect the actual actuation burden and the whole robots behaviour along curved trajectories. Therefore, it is interesting to estimate as precisely as possible the motors-to-wheels power flow to analyse the wheels slipping and their actual contribution to the robot dynamics.

Given the definition of $T_{\sim}$, and the need of modelling the transmission dynamics, the following generalized coordinates vector is considered:

$$\mathbf{x} = \begin{bmatrix} \mathbf{x}_f \\ \mathbf{x}_b \end{bmatrix} \tag{10}$$

where:

$$\mathbf{x}_{\sim} = \begin{bmatrix} x_{\sim} & y_{\sim} & z_{\sim} & \alpha_{\sim} & \beta_{\sim} & \gamma_{\sim} & \vartheta_{\sim,r} & \vartheta_{\sim,l} \end{bmatrix}^T \tag{11}$$

All of the coordinates contained in (11) have been defined already, with exception of $\vartheta_{\sim,r}$ and $\vartheta_{\sim,l}$ which are the rotation angles of the right and left motors respectively. The influence of such coordinates on the robot dynamics is described later as the transmission model is defined.

The potential energy V in (4) only considers the gravitational potential, since the vertical stiffness of the wheels is considered within the contact force model with ground. Considering as a reference the origin of the $r.f.\{0\}$, it is:

$$V = \sum_{\sim} m^*_{\sim} \mathbf{g}^T \mathbf{p}_{\sim} \tag{12}$$

with $\mathbf{g} = \begin{bmatrix} g_x & g_y & g_z \end{bmatrix}^T$, and $\|\mathbf{g}\| = 9.81\, ms^{-2}$. Varying properly the components of $\mathbf{g}$, it is possible to simulate differently sloped surfaces.

4.2 Kinematic Constraints

As aforementioned in the robots description, the class of articulated robots object of study is composed by a front and a back distinct parts connected by means of a universal joint. Such kinematic pair is composed of two revolutes with perpendicular axes which intersect in the connection point **O**. The first revolute is parallel to z axis of $\{f\}$; the second one is parallel to the x axis of $\{b\}$.

The resulting four constraint equations are:

$$\mathbf{\Phi} = \begin{bmatrix} \mathbf{p}_f + \mathbf{R}_f{}^{\{f\}}\mathbf{O}_f - \mathbf{p}_b - \mathbf{R}_b{}^{\{b\}}\mathbf{O}_b \\ \begin{bmatrix} 0 & 0 & 1 \end{bmatrix} \mathbf{R}_f^T \mathbf{R}_b \begin{bmatrix} 1 & 0 & 0 \end{bmatrix}^T \end{bmatrix} \tag{13}$$

where the first three ensure the coincidence of the points $\mathbf{O} \sim$ owned by the two modules, while the fourth constrains the two axes of the universal joint to remain perpendicular (i.e. z axis of $\{f\}$ and x axis of $\{b\}$).

Although it is not reported here for the sake of conciseness, the consequent Jacobian matrix $\mathbf{\Phi}_{\mathbf{x}}$ is obtained by differentiation of (13) as:

$$\mathbf{\Phi}_{\mathbf{x},ij} = \frac{\partial \mathbf{\Phi}_i}{\partial x_j} \tag{14}$$

which results in a 4×16 matrix.

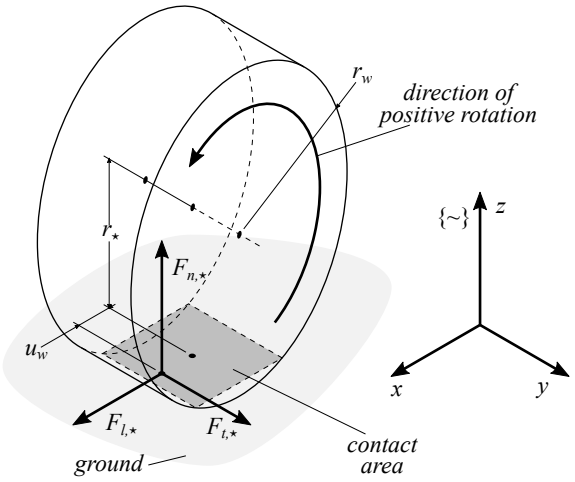

Fig. 4. Wheel-ground contact model

4.3 Wheels-Ground Contact Model

In order to simulate the wheels contact with ground, a simple model was used here; such model was already proposed and validated by authors in [25] for the Epi.q robot. The model takes into account the following phenomena:

- the longitudinal force exerted by the tyre on the ground, as a consequence of the wheel rotation; such force component is supposed proportional to the difference of velocity at the center of the contact area;
- a lateral force proportional to the velocity of the wheel body in the axial direction; this is the slipping force which is interesting to estimate for eight wheeled articulated robots, for whom this phenomenon is well evident;
- a vertical elastic force, proportional to the tyre deformation;
- a rolling resistance modelled as a non-symmetric distribution of the pressure within the contact area; such phenomenon results in a torque opposite to the rotation sense and it is formalized as a displacement in the longitudinal direction of the forces application point.

Referring to Fig. 4, the considered force components are computed as:

$$ {}^{\{\sim\}}\mathbf{F}_\star = \begin{bmatrix} F_{l,\star} \\ F_{t,\star} \\ F_{n,\star} \end{bmatrix} = \begin{bmatrix} k_l\,(r_w\omega_\star - \dot{p}_{x,\star}) \\ -k_t\,\dot{p}_{y,\star} \\ k_n\,(r_w - r_\star) \end{bmatrix} \tag{15} $$

where:

- the symbol $\star$ identifies each wheel of the articulated robot; a three letters codification is used from now, specifying which module of the robot (front and back, f and b), which wheels carrier of the module (right and left, r and l), and which wheel within the carrier (front and back, f and b); then, for example, the flb wheel indicates the wheel attached to the front module, to the left carrier, in back position;
- k_n, k_t and k_l vertical, transversal and longitudinal stiffness respectively; such parameters must be identified and strictly depend on the contact condition;
- $r_\star$ is the actual wheel radius, depending on the load applied on the $\star$ wheel;
- $\dot{p}_{x,\star}$ and $\dot{p}_{y,\star}$ are the longitudinal and transversal velocity components; even though they depend on the wheel attitude, their values were considered here just equal to those of the wheel attachment point to the carrier, which is an acceptable assumption for small roll angles $\alpha_\sim$;
- $\omega_\star$ is the wheel rotation rate; such value is directly related to the respective motor velocity introduced in (11) and it is specified later as a function of the transmission itself.

Due to the low velocities of the robots and the absence of an elastic suspensions system, the vertical dynamics of the wheels has been neglected. Nonetheless, given the relevance of wheels slipping in the dynamics of motion, the model was provided with a force saturation effect similar to the Coulomb classic frictional model. In particular, considering the horizontal force of each wheel $F_{h,\star} = \sqrt{F_{l,\star} + F_{t,\star}}$, the actual forces acting on the wheel-ground contact were modified as:

$$ F_{h,\star} > \mu_s F_{n,\star} \Rightarrow \begin{cases} F^*_{l,\star} = \mu_d F_{n,\star} \frac{F_{l,\star}}{F_{h,\star}} \\ F^*_{t,\star} = \mu_d F_{n,\star} \frac{F_{t,\star}}{F_{h,\star}} \end{cases} \tag{16} $$

The eight forces computed by (15) affect through the respective $\mathbf{Q}_\star$ vector, that can be obtained by the virtual works principle as:

$$ \delta\mathbf{x}^T\mathbf{Q}_\star = \delta\mathbf{p}_\star^T\mathbf{F}_\star \Rightarrow \mathbf{Q}_\star = \sum_i \frac{\partial \mathbf{p}_\star^T}{\partial x_i}\mathbf{F}_\star \tag{17} $$

where the vectors $\mathbf{p}_\star$ and $\mathbf{F}_\star$ must be expressed in the same reference frame, thus the actual orientation of each wheel shall be considered. For simplicity, it is chosen to disregard the pitch and roll rotations of the modules which marginally affect the force components. Therefore:

$$ \mathbf{Q}_\star = \sum_i \frac{\partial \mathbf{p}_\star^T}{\partial x_i}\mathbf{R}_{z,\gamma_\sim}\,{}^{\{\sim\}}\mathbf{F}_\star \tag{18} $$

The position of the forces application point can be easily computed as:

$$ \mathbf{p}_\star = \mathbf{p}_\sim + \mathbf{R}_{z,\gamma_\sim}\mathbf{R}_{x,\alpha_\sim}\,{}^{\{\sim\}}\mathbf{p}_\star \tag{19} $$

It should be noted that, for the wheels orientation, the pitch angle $\beta_\sim$ is disregarded since the wheels carriers are not subject to such rotation being connected to the chassis by means of a revolute joint parallel to y axis of the respective $r.f.\{\sim\}$.

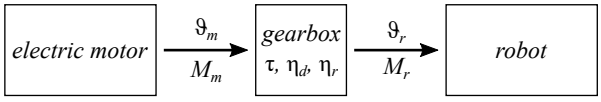

direct power flow: $\vartheta_m M_m \geq 0 \Rightarrow \eta_d \vartheta_m M_m = \vartheta_r M_r$

reverse power flow: $\vartheta_m M_m < 0 \Rightarrow \vartheta_m M_m = \eta_r \vartheta_r M_r$

Fig. 5. Functional scheme of the adopted power flow model

Also, the formulation can be further simplified with the assumption of small rotations $\alpha_{\sim}$.

The eight constant vectors ${}^{\{\sim\}}\mathbf{p}_{\star}$ are assumed as:

$$\begin{aligned}
{}^{\{\sim\}}\mathbf{p}_{\sim rf} &= \begin{bmatrix} \frac{i_{x,\sim}}{2} + u_w & \frac{-i_{y,\sim}}{2} & 0 \end{bmatrix}^T \\
{}^{\{\sim\}}\mathbf{p}_{\sim rb} &= \begin{bmatrix} \frac{-i_{x,\sim}}{2} + u_w & \frac{-i_{y,\sim}}{2} & 0 \end{bmatrix}^T \\
{}^{\{\sim\}}\mathbf{p}_{\sim lf} &= \begin{bmatrix} \frac{i_{x,\sim}}{2} + u_w & \frac{i_{y,\sim}}{2} & 0 \end{bmatrix}^T \\
{}^{\{\sim\}}\mathbf{p}_{\sim lb} &= \begin{bmatrix} \frac{-i_{x,\sim}}{2} + u_w & \frac{i_{y,\sim}}{2} & 0 \end{bmatrix}^T
\end{aligned} \tag{20}$$

The parameter u_w represents the displacement of the force application point related to the wheel rolling resistance. As known, such length is function of the contact parameters, and in particular of the wheel radius r_w and of the rolling resistance coefficient.

It is worth noticing that the four wheels and the origin of the $r.f.\{\sim\}$ were considered coplanar.

4.4 Transmission Model

As aforementioned, the transmission power flow is important for the modelling process of mobile robots with high number of wheels since their dynamic behaviour is strongly affected by the amount of slipping in the tyre-soil contact. To such aim, the power flow model schematically represented in Fig. 5 was adopted.

$$M_m - M_r \frac{\tau}{\eta} = \left(J_m + J_w \frac{\tau^2}{\eta} \right) \ddot{\vartheta}_m \tag{21}$$

where:

- M_m is the torque exerted by the motor;
- M_r is the torque generated by contact forces of the corresponding wheels; for the four motors it is:

$$\begin{aligned}
M_{fr} &= r_w \left(F_{l,frf} + F_{l,frb} \right) + u_w \left(F_{l,frf} + F_{l,frb} \right) \\
M_{fl} &= r_w \left(F_{l,flf} + F_{l,fl_b} \right) + u_w \left(F_{l,flf} + F_{l,fl_b} \right) \\
M_{br} &= r_w \left(F_{l,brf} + F_{l,brb} \right) + u_w \left(F_{l,brf} + F_{l,brb} \right) \\
M_{bl} &= r_w \left(F_{l,blf} + F_{l,bl_b} \right) + u_w \left(F_{l,blf} + F_{l,bl_b} \right)
\end{aligned} \tag{22}$$

- τ is the reduction ratio of the transmission;
- J_m and J_w respectively are the inertial parameters of the motor rotor, and of the attached wheels;

Table 3. Transmissions parameters of Epi.q and Agri.q

Parameter	Epi.q	Agri.q	
τ_f	1 : 205.00	1 : 47.64	$[-]$
τ_b	1 : 205.00	1 : 28.93	$[-]$
η_d	0.81	0.60	$[-]$
η_r	0.77	0.35	$[-]$

- η is the efficiency (< 1) of the transmission; such parameter assumes different meanings for direct and reverse power flows:

$$\begin{aligned}
M_m \dot{\vartheta}_m \geq 0 \Rightarrow \eta = \eta_d \\
M_m \dot{\vartheta}_m < 0 \Rightarrow \eta = \frac{1}{\eta_r}
\end{aligned} \tag{23}$$

  with η_d efficiency of the transmission when the power flows from the motor to the wheels, and η_r efficiency when the motor acts as a brake; such distinction is important because the difference among the values of η_d and η_r might be significant when the transmission ratio $\tau \ll 1$;
- ϑ_m is the motor angular acceleration.

Using (21), four equations can be found, one per each motor, to be added to the sixteen non trivial equations coming from (4). The reduction ratios of the Epi.q and Agri.q are shown in Tab. 3 and correspond to those actually available on the robots. The efficiencies η_d and η_r are reasonably assumed depending on the transmission architectures which are different for the two robots.

5 Model Analysis

To improve the understanding on the articulated robot dynamics, the model described in the previous section is analysed in the following. Due to its complexity, some simplifications are introduced by neglecting the less relevant terms, such as the roll and pitch angles, which are assumed null.

The effect of the back module on the robot manoeuvrability was evaluated in terms of its capability of affecting the whole system lateral and yaw accelerations. In particular, it must be kept in mind that the robot motion is controlled by means of the front module kinematics. Then, understanding what the effect of the actuation of the back driving units might be on the whole system means to understand how the forces exerted by the back wheels modify the dynamic behaviour of the front module.

To such aim, the dynamic equations introduced in the previous section can be solved, and the lateral and yaw accelerations ${}^{\{f\}}\ddot{y}_f$ and $\ddot{\gamma}_f$ can be considered. The influence of the contact forces generated by the actuation of the back

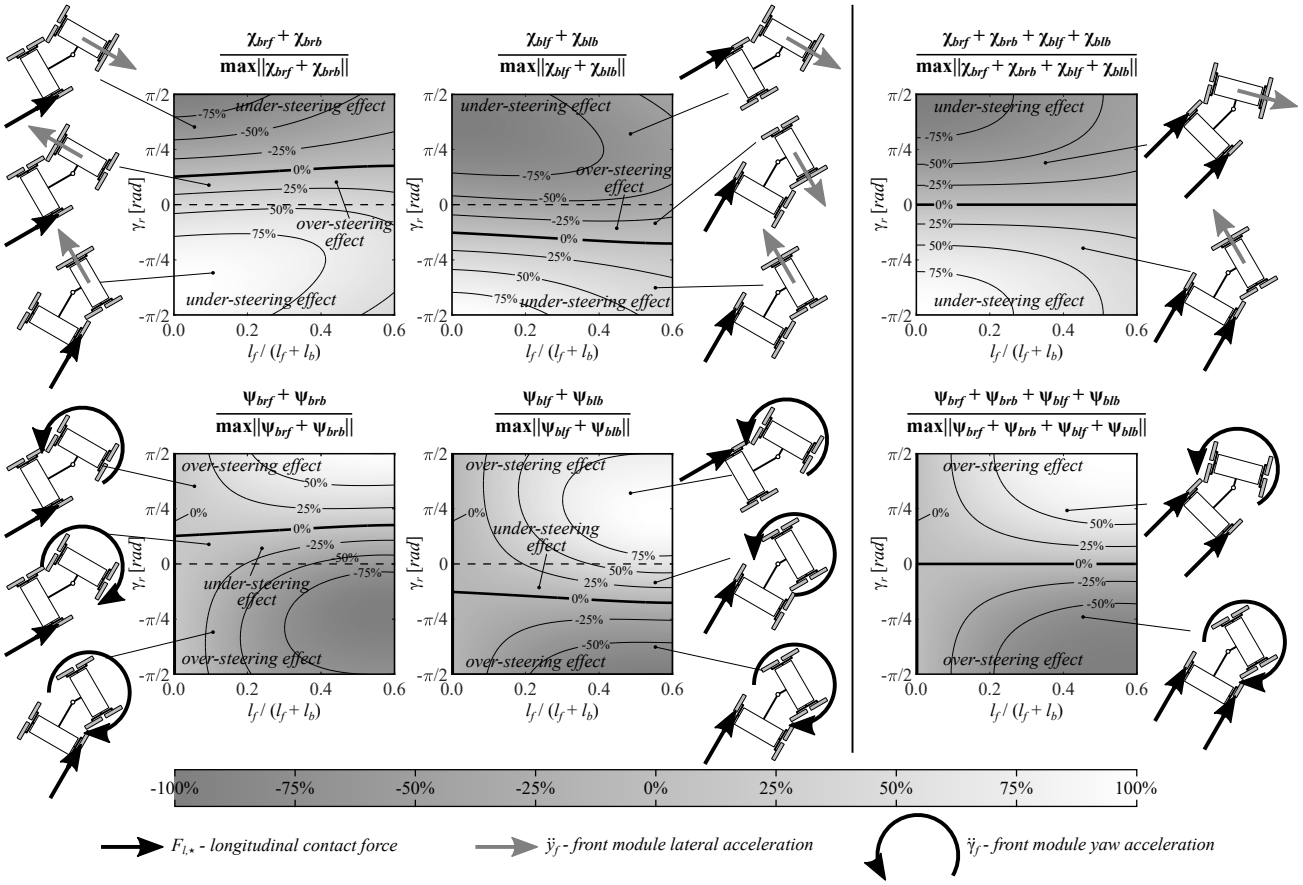

Fig. 6. Representation of the effect of the back driving units actuation on the dynamic behaviour of the articulated mobile robot: the maps on the right in particular show how the application of an equal torque to the back wheels of an articulated robot affect its ability to perform lateral and yaw accelerations only for Epi.q type robots, i.e. when $l_f/(l_f+l_b) > 0$

driving units can be then quantified by considering the terms:

$$\begin{aligned} \chi_\star &= \frac{\partial^{\{f\}}\ddot{y}_f}{\partial F_{l,\star}} = f\left(\gamma_\sim, i_{y,\sim}, l_\sim, r_w, m^*_\sim, J^*_{z,\sim}, J_w\right) \\ \psi_\star &= \frac{\partial\ddot{\gamma}_f}{\partial F_{l,\star}} = f\left(\gamma_\sim, i_{x,\sim}, l_\sim, m^*_\sim, J^*_{z,\sim}, J_w\right) \end{aligned} \tag{24}$$

The partial derivatives in (24) depends on almost all the robot geometrical and inertial parameters and their expression is too extended for been reported here. Nonetheless, it is possible to perform a numerical analysis on some relevant parameters and assuming reasonable values for the remaining. For example, the Fig. 6 graphically shows the results obtained for an articulated robot owning the Agri.q inertial properties. The values of the influence coefficients (24) have been let vary for different aspect ratios $l_f/(l_f+l_b)$, and a set of different relative yaw angles $\gamma_r = \gamma_f - \gamma_b$ were considered.

The maps in Fig. 6 yield some interesting conclusions:

- both right and left wheels provide a non-under steering contribution to the rover (characterized by $\chi_\star$ with same sign as γ_r) only for a small angle range, going from the line $\gamma_r = 0$ to the iso-curve $\chi_\star = 0$; the width of such range is affected by the rover aspect ratio l_f/l_b and, in general, is wider for Epi.q-like robots, more than for Agri.q ones;
- in approximately the same range of configurations, the actuation of the right and left wheels own a brake effect on the yaw acceleration, as evidenced by the sign of $\psi_\star$ which is opposite to that of γ_r: in other words, while the back actuation helps the forward module performing curved paths by providing centripetal accelerations, it also hinders the yaw accelerations $\ddot{\gamma}_f$ making necessary a higher actuation burden on the front module.

As done in automotive practice, it is useful provide the back wheels with equal torques in order to let them assess their angular velocities to those required by their paths, and letting the front module drive the whole trajectory. To such aim, it is interesting to observe what is the effect of an equal longitudinal force on right and left wheels, done here through the sum of the respective $\chi_\star$ and $\psi_\star$. Again from Fig. 6 one can conclude that:

- an equal longitudinal force on the back module wheels inevitably yields an under-steering effect on the front module (being the sign of the sum of $\chi_\star$ opposite to the sign of γ_r) at any configuration;
- the sign of the sum of $\psi_\star$ equals to the sign of γ_r suggesting that an equal force on the back module always improve the front module capability to modify its yaw orientation, lightening the front motors usage; however,

such effect is evident for robots having $l_f \sim l_b$, while is identically null when $l_f = 0$, i.e. for the rover Agri.q.

This last point deserves a particular attention since, as also pointed out later by simulations on the identified model, the obvious consequence is that the manoeuvrability of Agri.q cannot be improved by actuating the robot back actuators. Nonetheless, the use such motors can enlighten the burden of the front ones leaving their contribution essentially oriented at providing the front module with yaw accelerations (i.e. performing curves).

6 Numerical Implementation and Identification

The implementation of the dynamics equation followed the classical approach for algebraic systems, through an augmented mass matrix build up to contemporary solve the accelerations problem together with the kinematic constraint equations:

$$\begin{bmatrix} \mathbf{M} & \boldsymbol{\Phi}_{\mathbf{x}}^T \\ \boldsymbol{\Phi}_{\mathbf{x}} & \mathbf{0}_{4\times4} \end{bmatrix} \begin{bmatrix} \ddot{\mathbf{x}} \\ \boldsymbol{\lambda} \end{bmatrix} = \begin{bmatrix} \mathbf{n} \\ -\dot{\boldsymbol{\Phi}}_{\mathbf{x}}\dot{\mathbf{x}} \end{bmatrix} \tag{25}$$

where vector $\mathbf{n}$ collects all the terms not dependent on the coordinates accelerations.

Bearing in mind the final aim of the modelling process, which is that of simulating the articulated robots while performing different kind of trajectories, the desired velocity profiles of the front motors where provided in form of constraint equations as:

$$\boldsymbol{\Phi}^* = \begin{bmatrix} \vartheta_{fr} - \vartheta_{fr,d} \\ \vartheta_{fl} - \vartheta_{fl,d} \end{bmatrix} \tag{26}$$

Using a Baumgarten type formulation to ensure the following of non-continuous accelerations profiles, the constraint becomes

$$\ddot{\boldsymbol{\Phi}}^* + 2A\dot{\boldsymbol{\Phi}}^* + B\boldsymbol{\Phi}^* = \mathbf{0} \tag{27}$$

where the two parameters A and B where then set up to ensure the constraints fulfilment. The resultant differential algebraic system of equations assumes the form:

$$\begin{bmatrix} \mathbf{M} & \begin{bmatrix} \boldsymbol{\Phi}_{\mathbf{x}} \\ \boldsymbol{\Phi}_{\mathbf{x}}^* \end{bmatrix}^T \\ \begin{bmatrix} \boldsymbol{\Phi}_{\mathbf{x}} \\ \boldsymbol{\Phi}_{\mathbf{x}}^* \end{bmatrix} & \mathbf{0}_{6\times6} \end{bmatrix} \begin{bmatrix} \ddot{\mathbf{x}} \\ \boldsymbol{\lambda} \\ -M_{fr} \\ -M_{br} \end{bmatrix} = \begin{bmatrix} \mathbf{n} \\ -\dot{\boldsymbol{\Phi}}_{\mathbf{x}}\dot{\mathbf{x}} \\ -\dot{\boldsymbol{\Phi}}_{\mathbf{x}}^*\dot{\mathbf{x}} - 2A\dot{\boldsymbol{\Phi}}^* - B\boldsymbol{\Phi}^* \end{bmatrix} \tag{28}$$

where M_{fr} and M_{fl} are the actuation torques needed to follow the desired path constrained by (27).

The four equations coming from (21) also provide a further algebraic loop, for the values of the efficiency parameter η of each one of the four transmissions depend on the actual values of motors torques and angular velocities. In this approach, the model was simplified as shown in Fig. 8 by just

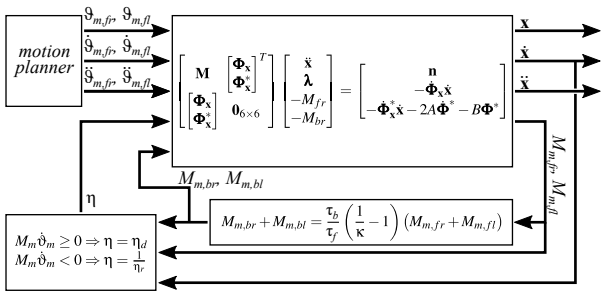

Fig. 7. Numerical implementation of the articulated robots dynamics model

considering in the numerical integration process the value of η at each step given by the power-flow at the previous integration step.

A similar feedback approach was also used for the motor torques M_{br} and M_{bl} fed to the back module, whose values can be determined according to different control laws. A simple, yet effective, approach can be that of dividing the whole torque exerted by the robot wheels with a given proportionality among front and back modules:

$$\sum_f M_{w,\star} = \kappa \sum_{\sim} M_{w,\star} \tag{29}$$

where $M_{w,\star}$ is the torque exerted by the single wheel. Given the transmission parameters described before, then it is:

$$M_{m,br} + M_{m,bl} = \frac{\tau_b}{\tau_f}\left(\frac{1}{\kappa} - 1\right)\left(M_{m,fr} + M_{m,fl}\right) \tag{30}$$

In other words, when $\kappa = 1$ the torque exerted by back module wheels is null and all the actuation effort burdens on the front wheels; when $\kappa = 0.5$ the contribution of front and back modules are equal. Given the transmission reductions and the motors characteristics, the actual range for of such parameter for Agri.q is $0.62 \leq \kappa \leq 1$, since the lower bound avoids the back motors exceeding their maximum working torque. Such constraint is not valid for Epi.q, whose modules are provided with equal modules and transmissions.

The model proposed and widely discussed in the previous part of the manuscript was validated through experimental tests for both the two prototypes Epi.q and Agri.q. Details on the parameters identification involving the Epi.q were provided by authors in [25]. A similar approach was also adopted for the Agri.q rover, whose parameters are detailed in Tab. 4. Some details about the experimental campaign that has been carried out to identify the model kinematics and dynamics model previously derived are provided in the following. Given the Agri.q main task, which is that of monitoring vineyards and crops in general, the rover might be subject to a variety of use conditions. Soil unevenness and slopes, ground humidity, and presence of grass are just some examples of the external factors which can affect the robot behaviour. To predict an always valid set of parameters is

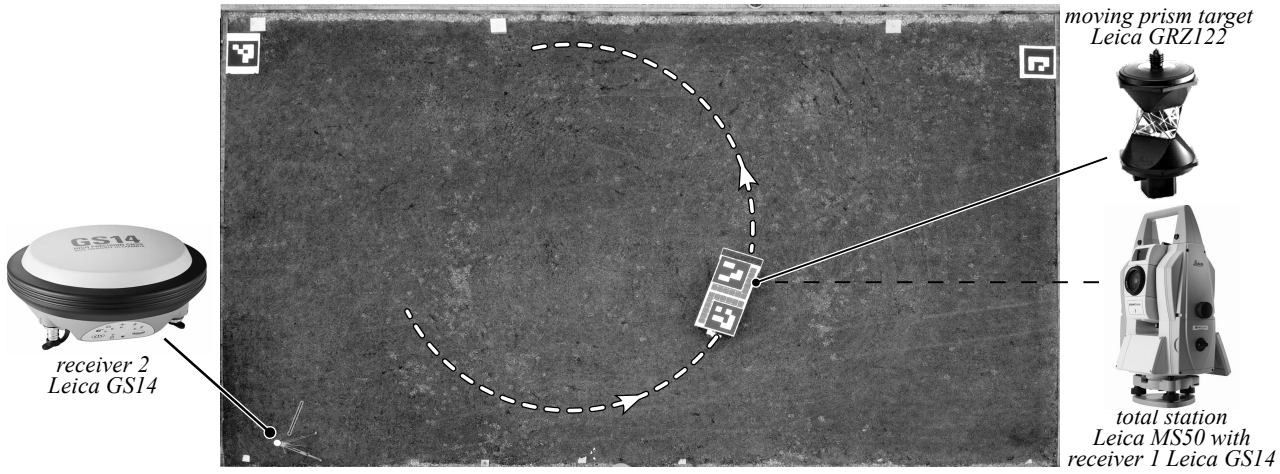

Fig. 8. Aerial view of the used test rig: Agri.q moving on a flat grassy surface having its trajectory captured by a Leica MS50 total station

impossible. Nonetheless, the model can still be exploited to design actuation strategies once it is validated on a significant application case.

The experimentation focused for this piece of research on identifying the Agri.q model in a quite simple condition: the tests were performed on a flat grassy surface, with limited unevenness. The rover was controlled to perform a circular trajectory at constant velocity going through the following steps:

- a transient acceleration phase with a cubic velocity profile characterized by a maximum acceleration $a_{max} = 0.5\,ms^{-2}$ in straight direction;
- a straight velocity section at constant cruise velocity v_c;
- a circular path with constant radius R and velocity v_c.

The values of the wheels rotations where computed by only considering the rover inverse kinematics, already tackled by authors in [25]. According to that approach, the wheels rotations where computed disregarding their slipping. As shown in the following, the actual behaviour of the robot is fundamentally different.

A set of experimentations were performed with different velocities and curve radius, moving the robot with different values of the division parameter κ. The tests were performed on a planar grassy field, similar to the expected rover work environment in terms of soil evenness. Due to the weather and humidity, the terrain was almost wet, offering a wide range of working conditions: from slippery spots with wet grass, to muddy points whith less dense turf. The robot actuation consisted in a planned reference trajectory fed to the forward actuation units. The velocity profiles generated as previously described were directly followed by the forward motors drivers; the back motors contributions were computed via (30). The acquired data-set was then used to identify the wheels contact parameters: the modelled articulated robot where moved by imposing the reference rotations in (28) equal to those recorded on the rover during the experimentations.

In order to perform a validation in term of positioning accuracy, a properly measured reference trajectory is required. This trajectory, used as ground truth, was captured by a total station (the Leica MS50 of Leica Geosystems AG, Heerbrugg, Switzerland) located on the vertices of a small georeferenced topographic network, tracing a moving 360° prism target (Leica GRZ122) mounted on the upper platform of the rover. Being the network geo-referenced, the components of the position of the prism also appear to be in the same reference frame. The geo-referencing of this network took place by locating two dual-frequency multi-constellation geodetic GNSS receivers (Leica GS14), in static acquisition for about an hour on the materialized vertices. The observations were subsequently post-processed with a differential approach and the network compensated in order to obtain the accurate coordinates of the points (cm-level accuracy) projected in a cartographic system (WGS84 reference system with the UTM32N projection). The layout of the test rig is shown in Fig. 8. The markers appearing in the picture were not used for this piece of research. The same experimental campaign, in fact, was exploited for calibrating a visual positioning system based on the use of UAVs (*unmanned aerial vehicles*).

Some comparative results in terms of planned motions, experimental and simulated paths and torques are shown in Fig. 9 for two trajectories not used in the identification process. The tests (here called Test 1 and Test 2) were performed at different cruise velocities (namely $0.5\,ms^{-1}$ and $1.0\,ms^{-1}$) and planned curve radius ($2\,m$ and $3\,m$ respectively). The parameters obtained by the identification process are collected in Tab. 4. As visible, the model fits with acceptable accuracy the actual paths and torques, and can be considered validated for the particular application scenario object of study, especially for low range velocities. Nonetheless, a huge deviation is recorded among the motion planning and the trajectory actually executed by the robot. This fact is attributable to at

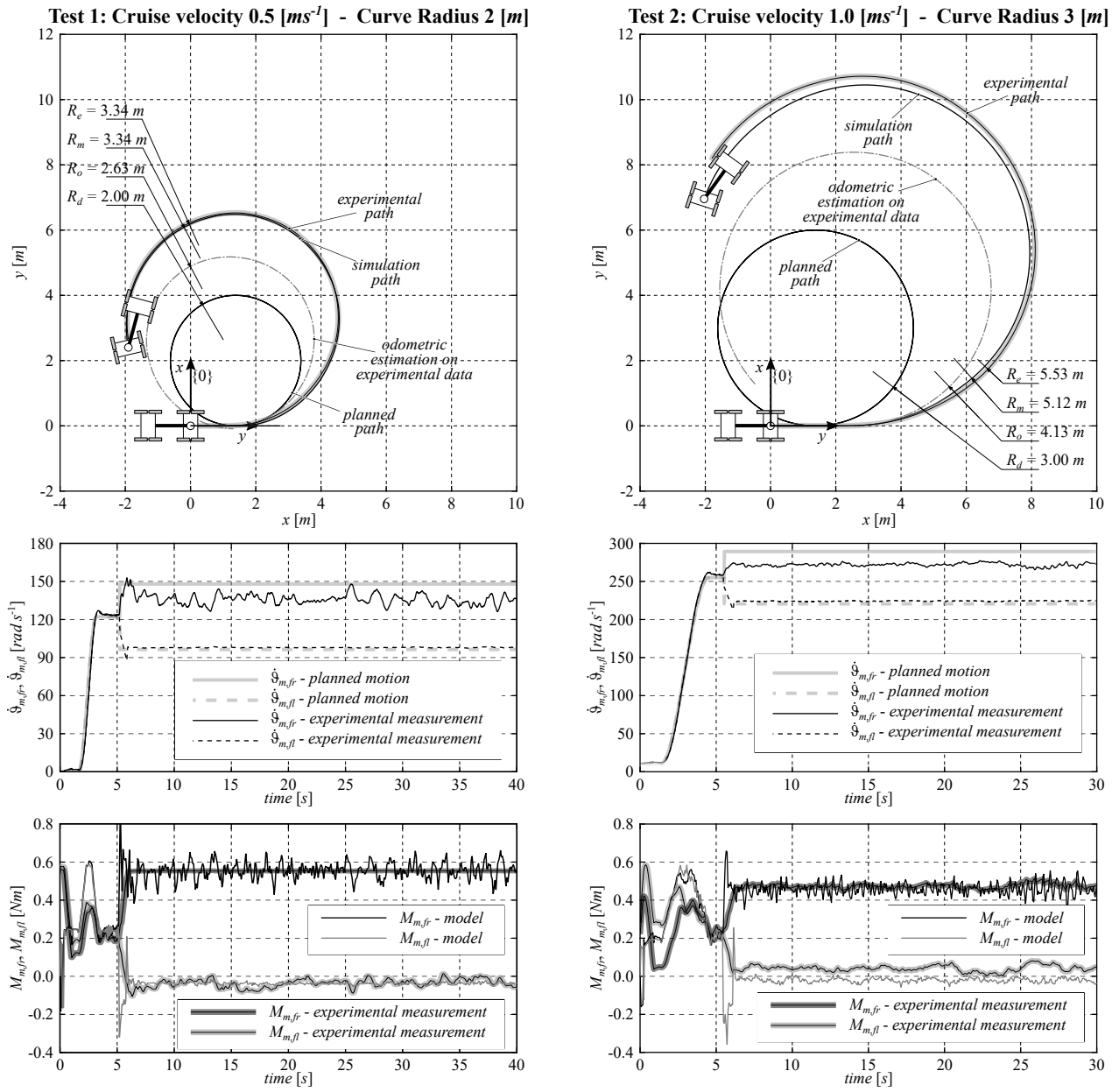

Fig. 9. Agri.q model validation: comparison among simulated and experimental variables for two trajectories with different radius and cruise velocity; Test 1 is performed at cruise velocity $0.5\,ms^{-1}$ and curve radius of $2\,m$, Test 2 at $1.0\,ms^{-1}$ and curve radius of $3\,m$

least two evident phenomena: on the one hand, the transversal contact forces acting on the wheels drive the robot far from a purely holonomic behaviour; on the other, the driving motors seem not able to follow with accuracy the reference velocity fed by the motion planner. This is well evident in both the $\dot{\vartheta}_{m,fr}$, $\dot{\vartheta}_{m,fl}$ curves shown in Fig. 9, and finds a justification in the torques graphs which show in both cases that the motor at the outer side of the curve reaches its upper thrust limit, preventing the right wheels to accomplish the desired motion.

In order to have a dimensionless parameter to compare the modelled and the experimental behaviours, the deviation from the desired pose was estimated through the error accumulated by the yaw angle γ_f of the front module while performing the motion. In particular, it was used e_γ, defined as:

$$e_\gamma = \frac{\int_0^{t_f} (\gamma_f - \gamma_d)\, dt}{\int_0^{t_f} \gamma_d dt} \tag{31}$$

where γ_d is the planned yaw angle, and t_f is the final instant of the simulated test. A second parameter defined to the aim of evaluating the performance is $e_{\mathbf{x}}$, which takes into consideration the Cartesian position of the front module:

$$e_{\mathbf{x}} = \frac{\|\mathbf{p}_f - \mathbf{p}_d\|}{\sigma} \tag{32}$$

Table 4. Relevant wheels contact parameters of Epi.q and Agri.q

Parameter	Epi.q	Agri.q	
k_l	200.00	2939.81	$[Nsm^{-1}]$
k_t	120.00	2039.05	$[Nsm^{-1}]$
k_n	11×10^3	15×10^3	$[Nm^{-1}]$
μ_s	0.90	0.63	$[-]$
μ_d	0.60	0.30	$[-]$
u_w	8.00×10^{-4}	8.32×10^{-3}	$[m]$

Table 5. Positioning error parameters in terms of yaw angle and Cartesian position of the front module for experimental and simulated trajectories

Parameter	Test 1	Test 2	
e_γ, experimental	-42.20	-48.69	$[\%]$
e_γ, simulation	-40.39	-43.77	$[\%]$
e_γ, odometric	-24.76	-30.81	$[\%]$
$e_\mathbf{x}$, experimental	24.02	16.45	$[\%]$
$e_\mathbf{x}$, simulation	24.30	14.33	$[\%]$
$e_\mathbf{x}$, odometric	3.53	5.05	$[\%]$

where $\mathbf{p}_d$ is the planned position of the front module at the end of the motion, and σ is the length of the planned path. The computed values of such parameters are collected in Tab. 5 for experimental, simulated and odometric results. As said, the external wheels are not able to perform the desired motion yielding an odometric estimation of the path very far from the planned one. The data in Tab. 5 basically confirm such behaviour, as demonstrated by the values of e_γ and $e_\mathbf{x}$. The difference among odometric estimation and experimental paths shows instead the effect of the wheels lateral forces on the trajectory: the robot is led to run even larger curves with postioning and orienting errors which increase also with cruise velocity and curve radius. Nonetheless, a pretty promising overlapping is shown by experimental and simulated data that demonstrate a low mutual deviation.

The behaviour is probably more simply described by the radius of the circular paths run by the robot. Referring to the two tests shown in Fig. 9, the two desired planned radius are $R_d = 2\,m$ and $R_d = 3\,m$. Since the external wheels are not able to perform the desired velocities, the resulting odometric estimations of the path turn very far from R_d, in particular the mean values $R_o = 2.63\,m$ and $R_o = 4.13\,m$ are observed. The captured trajectory is still different from the expected one, due to the friction transversal forces of the wheels on the ground: the experimental mean values of $R_e = 3.34\,m$ and $R_e = 5.53\,m$ are recorded. The dynamic model was identified to overlap this effect, to approximate as much as possible the actual dynamics of Agri.q. After identification, the model offers a mean radius of $R_m = 3.34\,m$ for the $0.5\,ms^{-1}$ trajectory, and $R_m = 5.12\,m$ for the $1.0\,ms^{-1}$ trajectory. In conclusion, for high velocity (it is worth reminding that the upper velocity limit for Agri.q is about $1.2\,ms^{-1}$) the model tends to underestimate the actual curvature of the rover trajectory of about 7.4%. Nonetheless, the accuracy shown for lower motions makes the presented dynamics model a useful tool that will be exploited in the next section to analyse the effect of a the actuation of the back driving units on the whole machine manoeuvrability.

7 Simulations

In this section, the dynamics model of articulated mobile robots which has been carried out and identified in the first part of the manuscript is used to verify the actual effect of a back actuation on the robots manoeuvrability. To such aim, the model was specialized with the parameters till now described of the two prototypes Epi.q and Agri.q. Each model was then integrated on similar yet properly scaled trajectories, composed as it follows:

- a transient acceleration phase with a cubic velocity profile characterized by a maximum acceleration a_{max} in straight direction;
- a straight velocity section of length s at constant cruise velocity v_c;
- a constant radius R and velocity v_c path for an angular distance of $\frac{3}{2}\pi$ in counterclockwise direction;
- a constant radius R and velocity v_c path for an angular distance of $\frac{3}{2}\pi$ in clockwise direction;
- a straight velocity section of length s at constant cruise velocity v_c;
- a transient deceleration phase with a cubic velocity profile characterized by a maximum value $-a_{max}$ in straight direction.

The two trajectories for Epi.q and Agri.q are detailed in Tab. 6, and the resulting simulations are shown in Fig. 10. Exactly as it is done with the actual prototypes, the desired motors velocities are forwarded to the driving units, without any feedback on the robot actual pose. The calculations were repeated for different values of κ, in particular for $\kappa = 1$ (back motors non active), $\kappa = 0.8$ (80% of the traction effort performed by the front module) and $\kappa = 0.6$ (60% of the traction effort performed by the front module). The cruise velocities chosen for the two robots represent the maximum performance of the respective prototype. Since the inertial effects on the robots behaviours increase with such parameter, this choice allows analysing the worst possible working condition in this sense.

As visible, neither Epi.q nor Agri.q are able to follow with precision the desired trajectory due to the absence of external feedback compensating the effect of the lateral forces acting on the wheels. It is worth noticing that, without simulated torque limits, the front module wheels precisely fol-

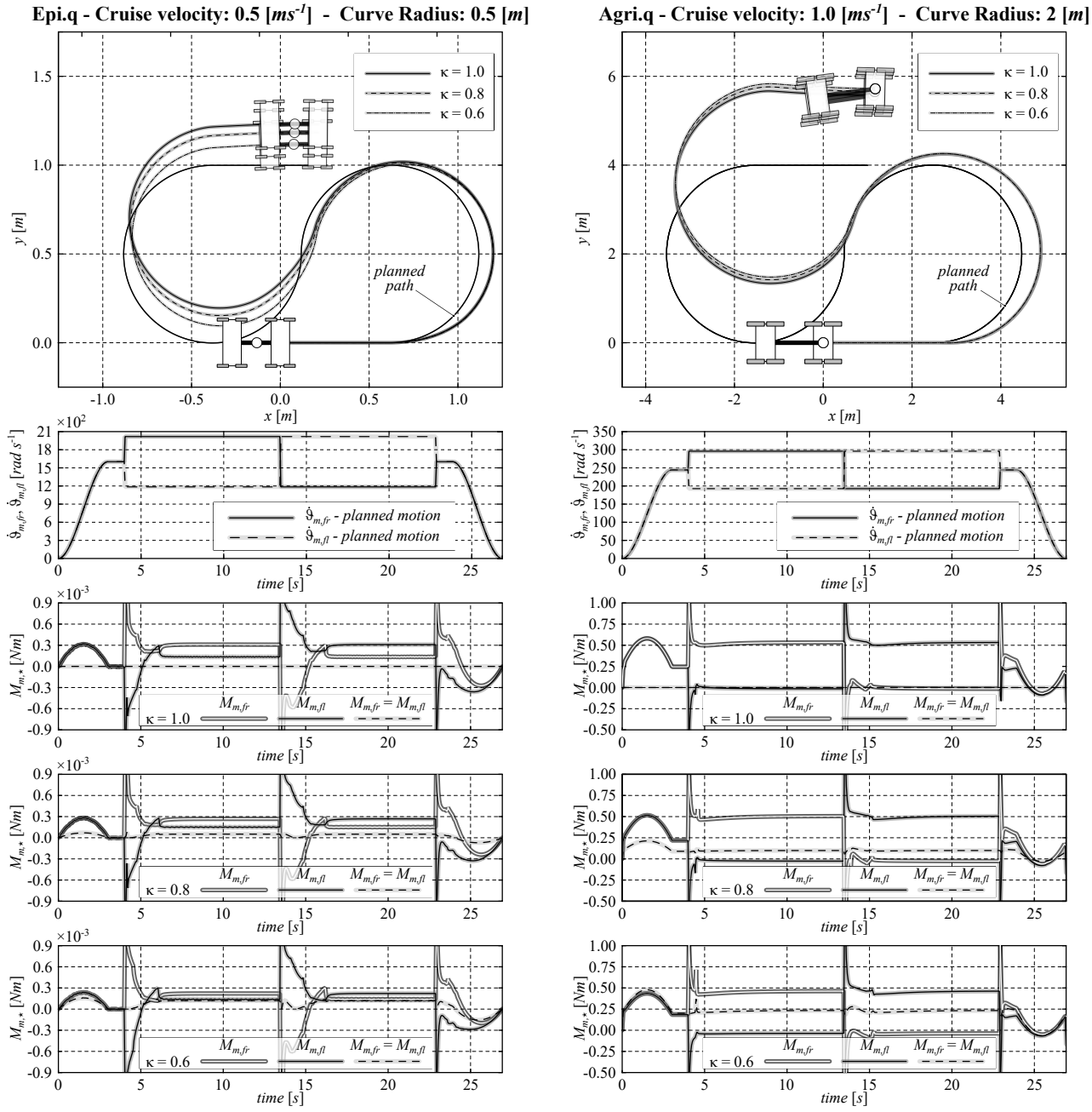

Fig. 10. Simulation performed on Epi.q and Agri.q models for evaluation of back driving effect; quantitative details on the paths are given in Tab. 6

low the planned velocity profile. The two performance parameters already introduced in (31) and (32) are used again to provide a quantitative comparison among the trajectories. The results, computed among the planned and the executed trajectories with different κ, are collected in Tab. 7. As visible from such parameters, and from the representations of Fig. 10, the actuation of the back module yields an improvement of the capacity of the articulated mobile robots to follow curved trajectories. It is worth remarking that the inertia of the robots should affect their behaviour as the velocity increases. Actually, due to the low dynamics of both the prototypes, such effects are negligible with respect to the contact with ground. Anyhow, the simulations were performed at the prototypes maximum allowed velocities in order to depict the worst possible working condition.

The most important improvement is obtained in terms of traction effort. In fact, it is possible to appreciate for both Epi.q and Agri.q that the actuation on the back driving units lightens the front motors from part of their burden. This is important in particular for the rover Agri.q which experimentally showed a critical behaviour while approaching curves due to the physical limits of its motors. Thus, the use of a back actuation can indirectly enhance the manoeuvrability for it demands the traction effort (or part of it) to the back motors while the torque exerted by the front motion units can be oriented at modifying the front module orientation, i.e. at

Table 6. Parameters of the simulated trajectories for parameters of Epi.q and Agri.q

Parameter	Epi.q	Agri.q	
R	0.50	2.00	$[m]$
s	0.50	2.00	$[m]$
v_c	0.50	1.00	$[ms^{-1}]$
a_{max}	0.25	0.50	$[ms^{-2}]$

Table 7. Positioning error parameters in terms of yaw angle and Cartesian position of the front module

Parameter	Epi.q	Agri.q	
$e_\gamma(\kappa = 0.6)$	1.98	4.36	$[\%]$
$e_\gamma(\kappa = 0.8)$	2.13	4.52	$[\%]$
$e_\gamma(\kappa = 1.0)$	2.52	5.10	$[\%]$
$e_\mathbf{x}(\kappa = 0.6)$	1.79	5.63	$[\%]$
$e_\mathbf{x}(\kappa = 0.8)$	2.20	6.83	$[\%]$
$e_\mathbf{x}(\kappa = 1.0)$	2.75	6.45	$[\%]$

performing curves. On the other hand, this effect is almost irrelevant for Epi.q, for whom however the beneficial effect of the back actuation lies on its improved ability to approach curves.

8 Conclusions

In the last decade, the use of mobile robots drew the attention of both research community and industry, for their versatility and breadth of applications. Among them, articulated robots play a special role for their innate modularity and scalability. It is the case of the Epi.q and Agri.q mobile robots, which are the main object of this piece of research. The main strength of these two robots is given by the high number of wheels they are provided with, which makes them particularly able to engage uneven grounds and to overpass obstacles. Unfortunately, such plus, also yields high parasitic contact forces which stray the actual behaviour from the kinematic one. This paper analyses such phenomenon, with particular attention to the beneficial effects than can be carried by a distributed locomotion effort. In first place, a reliable dynamics model is built and its parameters are experimentally identified. Such validation entitles the model to be used as a design tools for locomotion strategies of the tackled class of robots. At last, a simple strategy is tested in simulations for the two prototypes, to verify if the actuation of the back module wheels is actually beneficial to the robots manoeuvrability. As pointed out by the simulations, the use of back actuation can be of crucial importance even if the rover are not approaching sloped surfaces. For the Agri.q rover, due to the amount of wheels slipping, it was observed that the motors might not be able to provide the sufficient torque to run curved paths. The intervention of the back actuation helps to maintain an acceptable burden of the actuators, beneficially affecting the behaviour in curve although the theoretical effect shall be that of reducing the rover capacity to approach curves. The different geometry of the Epi.q robot makes such effect even more evident.

It is worth remarking that the proposed approach is valid for the tested workspaces of the two prototypes, for which the identified parameters are valid. Due to the extreme variability of the contact parameters, the quantitative results obtained by simulations should be considered valid only for applications of the same type (soil condition and evenness, mostly). Nonetheless, the correspondence among the validated model and the experimental data provide a reasonable level of confidence for considering it as an exploitable tool for testing of different actuation laws in simulated environment also with different wheels-ground contact parameters.

In conclusion, the combined use of experimental data and simulations helped to understand and quantify the actual advantage of using back actuation on articulated rovers. In future, the actuation strategies should evolve to enhance the robot behaviour, and to make the back motors intervene when required to accomplish the desired trajectories. Such growth can be prior tested in simulation environment thanks to the validated model object of this paper, and later on experimentally tested.

References

[1] Schneier, M., Schneier, M., and Bostelman, R., 2015. *Literature review of mobile robots for manufacturing*. US Department of Commerce, National Institute of Standards and Technology.

[2] Ortigoza, R. S., Marcelino-Aranda, M., Ortigoza, G. S., Guzman, V. M. H., Molina-Vilchis, M. A., Saldana-Gonzalez, G., Herrera-Lozada, J. C., and Olguin-Carbajal, M., 2012. "Wheeled mobile robots: a review". *IEEE Latin America Transactions,* **10**(6), pp. 2209–2217.

[3] Song, T., Xi, F. J., Guo, S., and Lin, Y., 2016. "Optimization of a mobile platform for a wheeled manipulator". *Journal of Mechanisms and Robotics,* **8**(6).

[4] Wei, Z., Song, G., Qiao, G., Zhang, Y., and Sun, H., 2017. "Design and implementation of a leg–wheel robot: transleg". *Journal of Mechanisms and Robotics,* **9**(5).

[5] Quaglia, G., Bruzzone, L., Oderio, R., and Razzoli, R. P., 2011. "Epi. q mobile robots family". In ASME International Mechanical Engineering Congress and Exposition, Vol. 54938, pp. 1165–1172.

[6] Quaglia, G., and Nisi, M., 2015. "Design and construction of a new version of the epi. q ugv for monitoring and surveillance tasks". In ASME Interna-

tional Mechanical Engineering Congress and Exposition, Vol. 57397, American Society of Mechanical Engineers, p. V04AT04A001.

[7] Visconte, C., Cavallone, P., Carbonari, L., Botta, A., and Quaglia, G., 2020. "Mechanism for the locomotion layout reconfiguration of the agri_q mobile robot". In International Conference on Robotics in Alpe-Adria Danube Region, Springer, pp. 390–399.

[8] Cavallone, P., Botta, A., Carbonari, L., Visconte, C., and Quaglia, G., 2020. "The agri. q mobile robot: Preliminary experimental tests". In The International Conference of IFToMM ITALY, Springer, pp. 524–532.

[9] Quaglia, G., Cavallone, P., and Lenzo, B., 2018. "On the dynamic analysis of a novel snake robot: preliminary results". In The International Conference of IFToMM ITALY, Springer, pp. 275–285.

[10] Quaglia, G., and Cavallone, P., 2018. "Rese_q: Ugv for rescue tasks functional design". In ASME International Mechanical Engineering Congress and Exposition, Vol. 52033, American Society of Mechanical Engineers, p. V04AT06A057.

[11] Kimura, H., and Hirose, S., 2002. "Development of genbu: Active wheel passive joint articulated mobile robot". In IEEE/RSJ International Conference on Intelligent Robots and Systems, Vol. 1, IEEE, pp. 823–828.

[12] Tanaka, M., Nakajima, M., Suzuki, Y., and Tanaka, K., 2018. "Development and control of articulated mobile robot for climbing steep stairs". *IEEE/ASME Transactions on Mechatronics,* **23**(2), pp. 531–541.

[13] David, J., and Manivannan, P., 2014. "Control of truck-trailer mobile robots: a survey". *Intelligent Service Robotics,* **7**(4), pp. 245–258.

[14] Granosik, G., 2014. "Hypermobile robots–the survey". *Journal of Intelligent & Robotic Systems,* **75**(1), pp. 147–169.

[15] Petrov, P., 2010. "Nonlinear backward tracking control of an articulated mobile robot with off-axle hitching". In Proc. WSEAS Int. Conf. ISPRA, pp. 269–273.

[16] Michałek, M., 2012. "Tracking control strategy for the standard n-trailer mobile robot–a geometrically motivated approach". In *Robot Motion and Control 2011*. Springer, pp. 39–51.

[17] Tanaka, M., Nakajima, M., and Tanaka, K., 2016. "Smooth control of an articulated mobile robot with switching constraints". *Advanced Robotics,* **30**(1), pp. 29–40.

[18] Murugendran, B., Transeth, A. A., and Fjerdingen, S. A., 2009. "Modeling and path-following for a snake robot with active wheels". In 2009 IEEE/RSJ International Conference on Intelligent Robots and Systems, IEEE, pp. 3643–3650.

[19] Tanaka, M., Tanaka, K., and Matsuno, F., 2014. "Approximate path-tracking control of snake robot joints with switching constraints". *IEEE/ASME transactions on mechatronics,* **20**(4), pp. 1633–1641.

[20] Tanaka, M., and Tanaka, K., 2016. "Singularity analysis of a snake robot and an articulated mobile robot with unconstrained links". *IEEE Transactions on Control Systems Technology,* **24**(6), pp. 2070–2081.

[21] Dhaouadi, R., and Hatab, A. A., 2013. "Dynamic modelling of differential-drive mobile robots using lagrange and newton-euler methodologies: A unified framework". *Advances in Robotics & Automation,* **2**(2), pp. 1–7.

[22] Corke, P. I., and Ridley, P., 2001. "Steering kinematics for a center-articulated mobile robot". *IEEE Transactions on Robotics and Automation,* **17**(2), pp. 215–218.

[23] Ali, S., 2017. "A unified dynamic algorithm for wheeled multibody systems with passive joints and nonholonomic constraints". *Multibody System Dynamics,* **41**(4), pp. 317–346.

[24] Classens, K., Koopaee, M. J., and Weiland, S., 2018. "Generalized dynamical modeling of 2-d modular snake robots". *Internship report, Eindhoven University of Technology, Eindhoven*.

[25] Botta, A., Cavallone, P., Carbonari, L., Tagliavini, L., and Quaglia, G., 2020. "Modelling and experimental validation of articulated mobile robots with hybrid locomotion system". In The International Conference of IFToMM ITALY, Springer, pp. 758–767.